BioMedical Engineering OnLine

BioMed Central

Research

Open Access

The relationship between wall shear stress distributions and intimal thickening in the human abdominal aorta

Michael Bonert[1,2], Richard L Leask[1,2,3], Jagdish Butany[4], C Ross Ethier[1,2], Jerry G Myers[1,2], K Wayne Johnston[2,5] and Matadial Ojha*[1,2]

Address: [1]Department of Mechanical and Industrial Engineering, University of Toronto, Canada, [2]Institute of Biomaterials and Biomedical Engineering, University of Toronto, Canada, [3]Department of Chemical Engineering, McGill University, Canada, [4]Department of Pathology, University Health Network and University of Toronto, Canada and [5]Department of Surgery, University Health Network and University of Toronto, Canada

Email: Michael Bonert - michael.bonert@utoronto.ca; Richard L Leask - richard.leask@mcgill.ca; Jagdish Butany - jagdish.butany@uhn.on.ca; C Ross Ethier - ethier@mie.utoronto.ca; Jerry G Myers - jerry.myers@grc.nasa.gov; K Wayne Johnston - kwjohnston@torhosp.toronto.on.ca; Matadial Ojha* - dyal.ojha@utoronto.ca

* Corresponding author

Published: 26 November 2003

BioMedical Engineering OnLine 2003, **2**:18

Received: 24 June 2003
Accepted: 26 November 2003

This article is available from: http://www.biomedical-engineering-online.com/content/2/1/18

Abstract

Purpose: The goal of this work was to determine wall shear stress (WSS) patterns in the human abdominal aorta and to compare these patterns to measurements of intimal thickness (IT) from autopsy samples.

Methods: The WSS was experimentally measured using the laser photochromic dye tracer technique in an anatomically faithful *in vitro* model based on CT scans of the abdominal aorta in a healthy 35-year-old subject. IT was quantified as a function of circumferential and axial position using light microscopy in ten human autopsy specimens.

Results: The histomorphometric analysis suggests that IT increases with age and that the distribution of intimal thickening changes with age. The lowest WSS in the flow model was found on the posterior wall inferior to the inferior mesenteric artery, and coincided with the region of most prominent IT in the autopsy samples. Local geometrical features in the flow model, such as the expansion at the inferior mesenteric artery (common in younger individuals), strongly influenced WSS patterns. The WSS was found to correlate negatively with IT (r^2 = 0.3099; P = 0.0047).

Conclusion: Low WSS in the abdominal aorta is co-localized with IT and may be related to atherogenesis. Also, rates of IT in the abdominal aorta are possibly influenced by age-related geometrical changes.

Background

Since the time of Virchow, approximately 150 years ago, it has been known that atherosclerotic lesions form at specific sites in the arterial tree, such as bifurcations, branch points and regions of curvature. The explanation for this localization is now generally regarded to be the result of abnormal wall shear stresses (WSS). Therefore, a considerable amount of work has focused on describing arterial hemodynamics in simplified and idealized vascular

Table 1: Patient-Specific Abdominal Aorta Model Geometry

	Model Inlet	Inferior of Renal BP	Minimum IR Dia.	IMA Ostium	Maximum IR Dia.	Aortic Bifurcation
Diameter†	1.00	0.84	0.75	0.79	0.83	0.81
Location*	0.0	3.3	4.7	5.3	6.0	7.5

† – Hydraulic Diameter [34] (in centimeters), * – Distance from Model Inlet (in centimeters), BP – Branch Point, IMA Ostium – Inferior Mesenteric Artery Ostium, IR Dia. – Infrarenal (Hydraulic) Diameter.

models [1]; here we focus on the hemodynamic patterns in the abdominal aorta [2-10].

It is known that WSS patterns depend on a sensitive way on arterial geometry. The abdominal aorta geometry varies significantly between individuals and is dependent on sex and age [11-15]. Previous hemodynamic studies on the abdominal aorta have primarily focused on older individuals. However, it is important to examine the hemodynamic factors that are present in younger individuals since they are likely to indicate the precursors to the continual progression of aortic vascular disease exhibited in the elderly.

The hemodynamics of the abdominal aorta inferior to the renal arteries have not been studied in detail in a young anatomically faithful patient-specific model, nor has a detailed map of intimal thickening in the abdominal aorta been made for the young and old. The objective of this work was to measure the WSS in a model of a normal human abdominal aorta and to determine the relationship between WSS and intimal thickness (IT) measured in human aorta autopsy samples. Of specific interest were the locations of areas with large intimal thickening (in autopsy samples) and regions with low WSS and with high spatial WSS gradients (*in vitro* flow model). We focused on WSS and spatial gradient of WSS since these hemodynamic factors have been shown to alter vascular cell function and morphology [16-18] and have been putatively linked to the development of atherosclerosis [19-22].

Methods and Materials

Construction of an Anatomically Faithful Flow Model

The anatomically faithful flow model of a normal human abdominal aorta was made in the following six steps: (1) performing a CT scan, (2) constructing a computer model, (3) making a (scaled) stereolithography model, (4) constructing a mould, (5) making an alloy replica and then (6) producing the flow model.

A CT-scan/angiogram was performed on a healthy 35-year-old male. The 287 axial slices within the region enclosing the abdominal aorta and iliac arteries were output in jpeg format, from which the cross-sectional contours of the aorta and its branches were isolated and smoothed using software written in the MATLAB programming environment (MathWorks, Natick, MA) using previously published techniques [23]. The slice and spacing data were then imported into a commercial CAD package (DDN, ICEM-CFD, Berkeley, CA) to create a computer model of the lumen-wall boundary using 3-D spline surfaces. This surface data was scaled so that the inlet diameter of the model was 1.00 cm, to optimize the model for flow visualization. The scaled data was then exported in the IGES file-format and sent to a rapid prototyping contractor (Factotum Plastics, Mississauga, ON) to make a stereolithography model. Selected geometrical characteristics of the model are presented in Table 1.

A flexible silicone mould (Sylgard® 182; Dow Corning, Midland, MI) was made using the stereolithography model as positive. This negative mould was then used to make a replica of the stereolithography model by melting a low melting point alloy (Cerrolow®-117, Cerro Metal Products, Bellefonte, PA), injecting it into the mould, and allowing it to cool. Prior to injection, two copper stringers were suspended in the centre of the lumen, from the cranial end to the caudal end, to mechanically reinforce the alloy model. Once solidified, the alloy cast was polished to produce a smooth surface without surface imperfections. The four exit branches (bilateral internal and external iliac arteries) of the final alloy model were extended with circular sections using additional alloy metal. This ensured that the outlets were not obscured by the outlet attachment segments. Also, the inlet was extended and a gradual transition was made from the inlet of the model (which is near circular) to a circular cross-section. Based on diameter measurements at the inferior mesenteric artery (IMA) of the computer model (CAD surface) and flow model, the error associated with the making of the flow model was estimated to be less than 3%. Steps 4–6 have been used previously in our lab and are described in more detail by Kirpalani [24] and Park [24,25].

Flow Rates and Flow Rate Validation

We studied hemodynamic patterns under steady flow conditions corresponding to mean flow at rest and during mild exercise [3,10]. In order to ensure physiologic hemodynamic conditions within the model, it was necessary to

Table 2: Reynolds number, flow rate and *in vivo* WSS by physiological condition.

Physiological condition	Reynolds number	Scale model volumetric flow rate	Hagen-Poiseuille *in vivo* WSS at the IMA†
Rest	227	2.68 mL/s	0.879 dyn/cm^2
Mild Exercise	757	8.93 mL/s	2.932 dyn/cm^2

† – Values for Hydraulic Diameter of 18.7 mm.

match the Reynolds numbers in the model with the mean Reynolds number *in vivo*. In turn, this required a reference diameter. The focus of the hemodynamic investigation was the infrarenal segment of the aorta and the abdominal aortic bifurcation, so we took the hydraulic diameter of the aorta at the level of the IMA to be the reference diameter. Direct measurement on the model gave this value as 7.94 millimetres, compared to the corresponding *in vivo* hydraulic diameter of 18.7 millimetres [3]. The remaining parameters necessary for the scaling calculation were the working fluid kinematic and dynamic viscosities ($1.89 \times 10^{-6} m^2/s$ and 1.43×10^{-3} kg/(m s)) [26] and blood kinematic viscosity, which was assumed to be independent of shear rate and equal to $4.0 \times 10^{-6} m^2/s$ [27]. The required model flow rates and the corresponding *in vivo* WSS values are given in Table 2, where WSS values are calculated from Poiseuille flow in a tube of diameter equal to the specified hydraulic diameter.

Wall Shear Stress Measurements

The laser photochromic dye tracer technique set-up has previously been validated against analytical and numerical solutions of the Navier-Stokes equations [25,28]. and has been used to measure complex arterial flows [20,24,29,30]. Fluid displacement profiles and WSS were analysed for the left and right midcoronal (or midfrontal) sections and the left and right midsagittal sections (Figure 2 and Figure 3, respectively). The midcoronal sections and midsagittal sections are approximately planar and include the left and right walls *and* the anterior and posterior walls respectively (Figure 1). To accomplish this, approximately 4000 traces were obtained and reviewed. WSS data was smoothed using the 'csaps' function in MATLAB, a hybrid weighted cubic smoothing spline and least squares fitting routine. The WSS axial gradient was calculated by numerical differentiation of the smoothed WSS data (Figure 2 and Figure 3) using a 2nd order central difference formula for unequally spaced data.

Histomorphometry

Histological specimens were prepared from ten abdominal aortas obtained at autopsy, typically within 48 hours of death. Donor information is shown in Table 3. The mean age of the subjects was 41.3 ± 20.6 (mean ± standard deviation) years.

All aortas were fixed unpressurized in 10% formalin for at least 48 hours, after blood and thrombi were removed. The remaining connective tissue around the aorta was then carefully removed using blunt dissection. The samples were oriented using the major branches (celiac, superior mesenteric artery (SMA), and renals) and the aortic bifurcation. To mark the orientation of the aortas, surgical sutures (2.0 Braided Silk – Black (K-832), Ethicon Inc., Somerville, NJ) and India ink were used. The India ink was used to mark the anterior surface of the aorta and the sutures (in the adventitia or media) the left or right side. At the bifurcation two sutures were used on one side so that left and right could be easily differentiated.

Aortas with calcification were decalcified for 3–5 hours using Rapid Bone Decalcifier for the Preparation of Histological Materials (Apex Engineering Products Corp., Plainfield IL) to facilitate sectioning. Axial cross sections were taken at approximately 4–5 millimeter intervals and then embedded in paraffin, sectioned and stained with a Verhoff elastic-Masson trichrome stain.

For the purpose of the histomorphometric analysis, the specimens were divided into eight axial regions (See 'Schematic' on Figure 5). These axial regions were subsequently subdivided into four circumferential regions (anterior, posterior, left and right). Histomorphometric measurements of intimal thickness were made from the internal elastic lamina to the edge of the lumen using the Leica QMC500 morphometric package, on a Leica DMRB photomicroscope (Leica, Toronto ON). Seven evenly spaced measurements, from the lumenal surface to the internal elastic lamina, were taken at each of the four circumferential positions, and subsequently averaged to obtain a representative value for each location. IT measurements in regions close to small branches were avoided. Over 12,000 measurements were made on over 450 slides.

Statistical Analyses

All statistical analyses were carried out with Prism 2.01 software (GraphPad Software Inc., San Diego CA). The different regions of the aortas were compared using ANOVAs and Bonferroni's multiple comparison. Also, linear

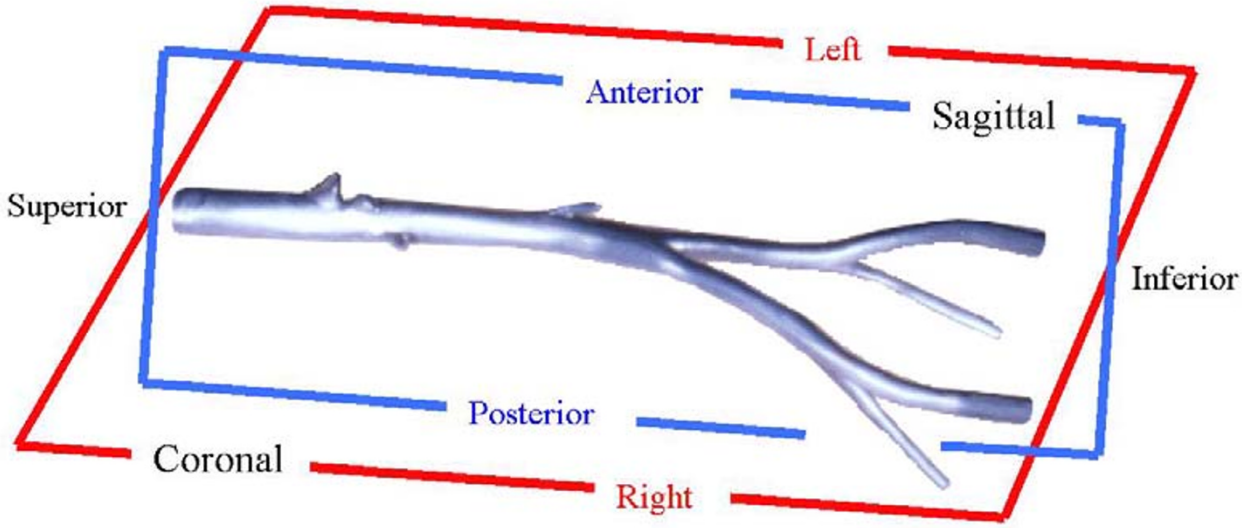

Figure 1
The alloy model of the abdominal aorta used for flow measurements. The midcoronal and midsagittal planes are shown.

regressions were done between age and IT. Findings that exhibited $P < 0.05$ were deemed statistically significant.

Results

Hemodynamics

Displacement Profiles

Figure 2 and Figure 3 show the digitized and smoothed displacement traces along the abdominal aorta flow model in the midsagittal and midcoronal sections for rest flow. Fluid displacement profiles in the midsagittal plane show that the high velocity fluid distal to the IMA travels closer to the wall with the greater curvature, the anterior wall, while the slower moving fluid is closer to the wall with the lesser curvature, the posterior wall (Figure 2). This suggests that significant secondary flows were present in the trunk of the aorta.

Since none of the displacement profiles exhibited negative displacements, it can be deduced that no regions of significant flow separation or flow reversal were present in the model for the flow conditions considered. The small displacements of the profiles at the posterior wall close to the bifurcation suggest that at higher Reynolds numbers a recirculation region may develop there (Figure 3).

Wall Shear Stress and Wall Shear Stress Gradient

The WSS and WSS axial gradient under resting conditions are shown in Figure 2 and Figure 3 for the midcoronal and midsagittal sections. WSS increased in the proximal region of the model until just proximal of the IMA. At the IMA region the WSS decreased along all the walls, with the largest decline on the posterior wall. This produced a WSS on the posterior wall that was minimum for the whole model. Just proximal to the abdominal aortic bifurcation the WSS on all walls increased. The posterior, anterior, left and right walls all experienced maximal WSS values a small distance distal to the abdominal aortic bifurcation. The largest WSS values were observed on the inner walls of the flow divider. The maximal WSS value overall was on the inner wall of the left common iliac (LCI) at the abdominal aortic bifurcation; this region also had the largest WSS spatial gradient in rest flow. Also, the WSS profile in the sagittal plane in mild exercise flow for the LCI posterior wall and LCI anterior wall were stretched in relation to the profile in rest flow; the WSS profile had lower WSS gradients than in rest flow. It was noted that for the exercise flow condition, the development length on the inner wall in the LCI was longer and the normalized peak WSS value lower. These effects were also present in the right common iliac (RCI), but were of much smaller magnitude (data not shown).

Histomorphometry

Qualitative Observations

The abdominal aortas of the two youngest subjects were generally characterized by thinner intimas. The greatest

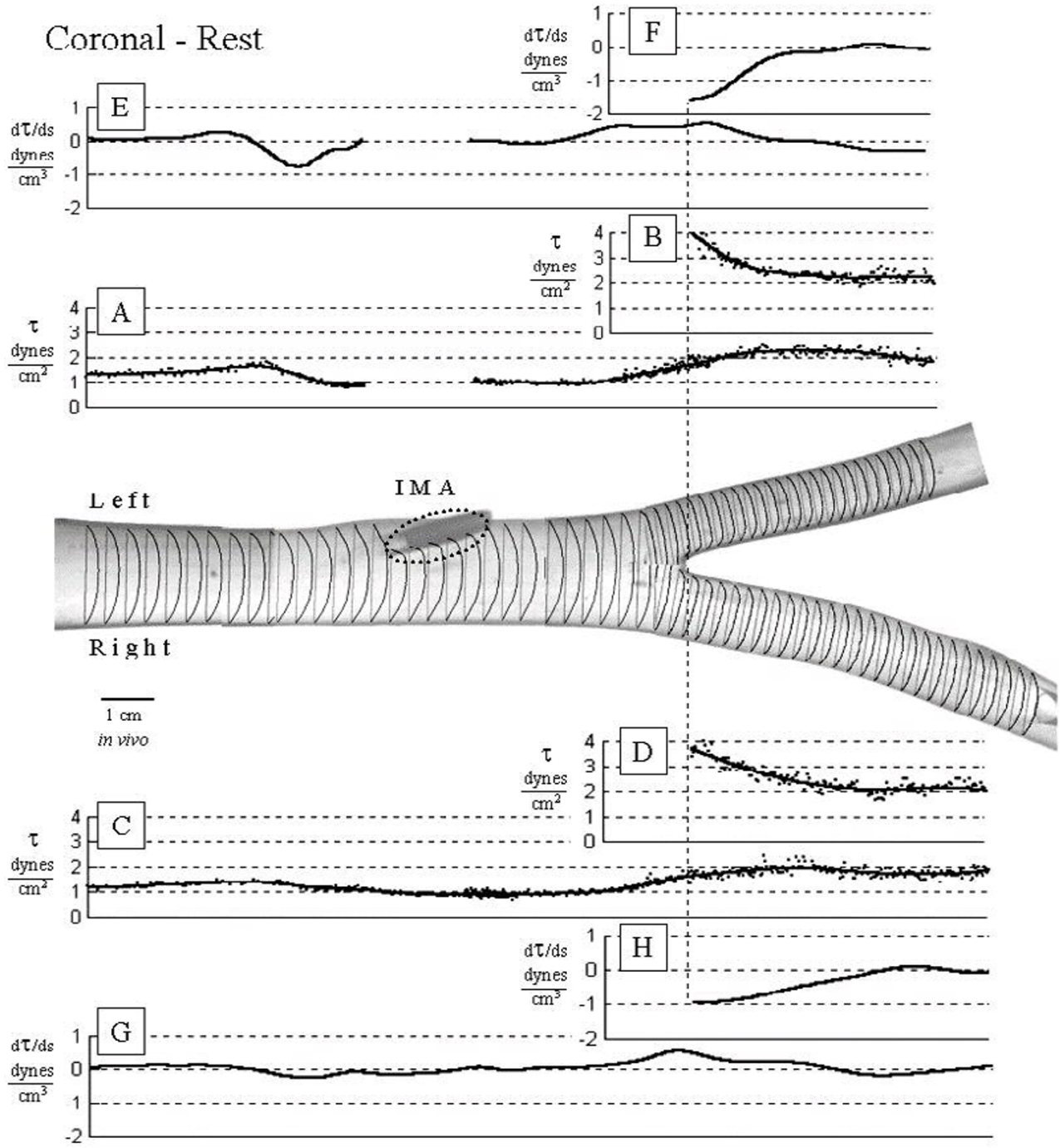

Figure 2
Midcoronal section displacement profiles, *in vivo* WSS (τ) in dynes/cm² (data points and curve fit) and calculated *in vivo* WSS spatial gradient (dτ/ds) in dynes/cm³ for resting flow. The pair of graphs at the top show the WSS along the left wall [A] and the inner wall [B] of the LCI (left common iliac). The pair of graphs at the very top show the WSS spatial gradient along the left wall [E] and the inner wall [F] of the LCI. The pair of graphs at the bottom show the WSS along the right wall [C] and the inner wall [D] of the RCI (right common iliac). The pair of graphs at the very bottom show the WSS spatial gradient along the right wall [G] and the inner wall [H] of the RCI. Profiles at the IMA (dashed oval) could not be resolved because of the IMA.

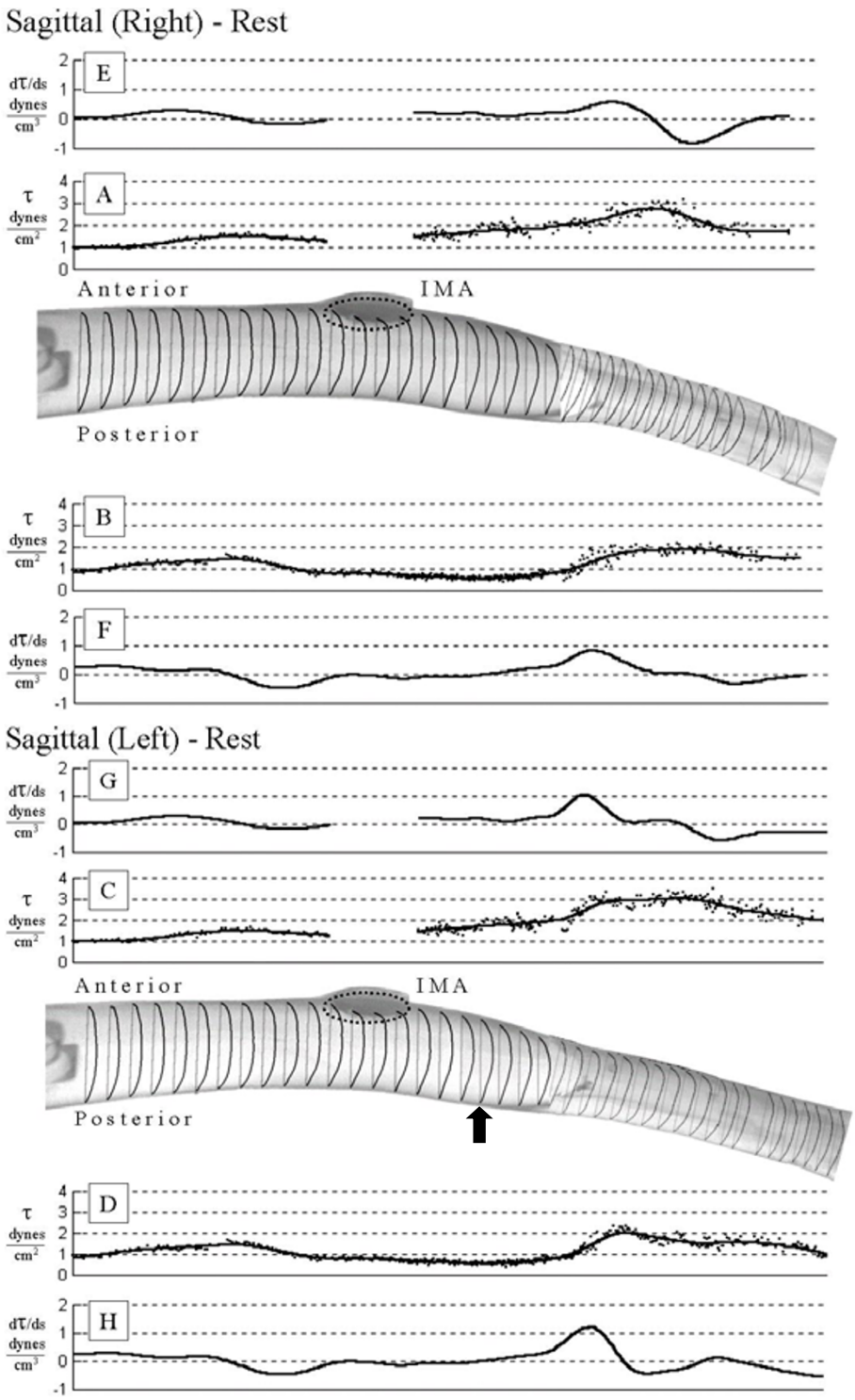

Figure 3
Right and left midsagittal section displacement profiles, *in vivo* WSS (τ) in dynes/cm^2 (data points and curve fit) and calculated *in vivo* WSS spatial gradient (dτ/ds) in dynes/cm^3 for resting flow. The graphs above the displacement profiles show the WSS [A] [C] and the WSS spatial gradient [E] [G] along the anterior wall. The graphs below the displacement profiles show the WSS [B] [D] and the WSS spatial gradient [F] [H] along the posterior wall. The solid arrow points to the region that exhibited the lowest WSS. Profiles at the IMA (dashed oval) could not be resolved because of the IMA.

Table 3: Aorta Samples – Details. Listed in the order of collection.

Case	Age	Sex	Cause of Death
S1	18.7	F	Systemic Lupus Erythematosus, Pericarditis, Tamponade
S2	27.9	F	Congenital Heart Disease /Rupture of R Pulmonary A
S3	32.1	F	Acute Pancreatitis /ARDS /Sepsis
S4	63.4	M	COPD, ARDS, CHF, Anemia
S5	45.9	F	Double Lung Transplant / Multiorgan Failure
S6	79.5	M	CAD Post AV Repair, Wound Sepsis, Post CABG, Cardiac Amyloidosis
S7	54.9	M	ARDS/Bilateral Acute Broncho-pneumonia/ Acute Heart Graft Rejection
S8	22.6	M	Acute Promyelocytic Leukemia / Sepsis
S9	48.8	M	Bullous Emphysema/ Tension Pneumothorax/ Cardiac Arrest/ Cerebral Anoxia
S10	19.3	M	Acute Lymphoblastic Leukemia / Acute Respiratory Failure

ARDS – Adult Respiratory Distress Syndrome, COPD – Chronic Obstructive Pulmonary Disease, CHF – Congestive Heart Failure, CAD – Coronary Artery Disease, AV – Aortic Valve, CABG – Coronary Artery Bypass Graft, R – Right, A – Artery.

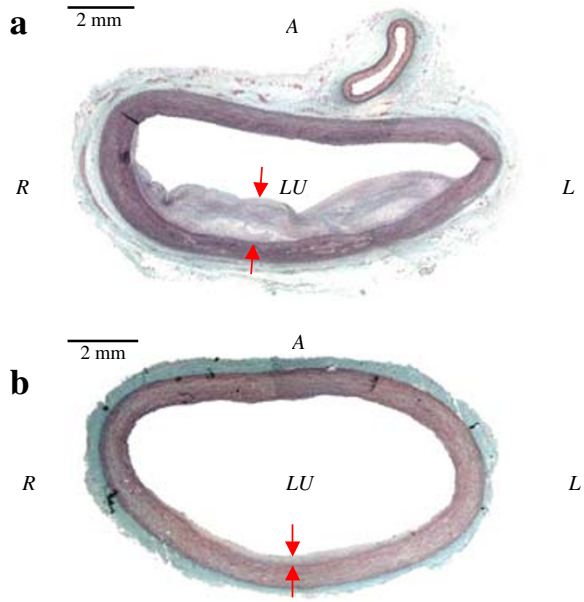

Figure 4
Abdominal aorta histologic cross sections (a) a short distance distal to the IMA ostium. S3, female, age 32.1 year old. The fibrous intima (purple/blue) is easily distinguished from the muscular media (red) (b) infraIMA region. S1, female, age 18.7 year old. Elastic trichrome stain. L – Left, R – Right, A – Anterior, LU – Lumen. The pairs of arrows denote the intimal thickness on the posterior wall.

intimal thickening was found in infraIMA region, and more specifically on the posterior wall (Figure 4). Other regions in these subjects exhibited minimal intimal thicknesses.

A similar pattern was seen in the slightly older individuals (S3 and S5), who also had noticeably thicker intimas on the posterior wall of infraIMA region (Figure 4). The older subjects generally had considerably thicker intimas in all regions, and in comparison to the younger subjects exhibited considerably more thickening in the supraceliac region and branch region. The thickening in the infraIMA region was not prominent alone or when compared to other regions. In addition, the older subjects generally had more complicated lesions. For example, S9, a 49 year old, and S4, a 63 year old, both exhibited very complex lesions along the length of the abdominal aorta and common iliac arteries. S9 developed lesions on the flow divider wall and exhibited substantial medial thinning.

Statistical Analysis

Linear regression found a significant relationship between patient-specific mean IT and age. The coefficient of variation (r^2) of the regression was 0.5038 (P = 0.0215). The mean thickness was defined as the thickness of all the measurements taken in the branch region, infrarenal, and infraIMA sections; these values were used to normalize patient IT data and will henceforth be referred to as "patient-specific mean IT." The average of the patient-specific mean IT values for all the samples was 0.5149 mm and the range of these values was 0.069 mm to 1.395 mm. The relationships between normalized IT of the axial sections and age were also examined. The normalized IT by axial position was correlated with age for the supraceliac, branch region and infraIMA sections. The supraceliac and branch region sections had positive correlations (supraceliac: $r^2 = 0.5699$, P = 0.0116; branch region: $r^2 = 0.4713$ P = 0.0284). The infraIMA had a negative correlation (infraIMA: $r^2 = 0.5771$, P = 0.0108).

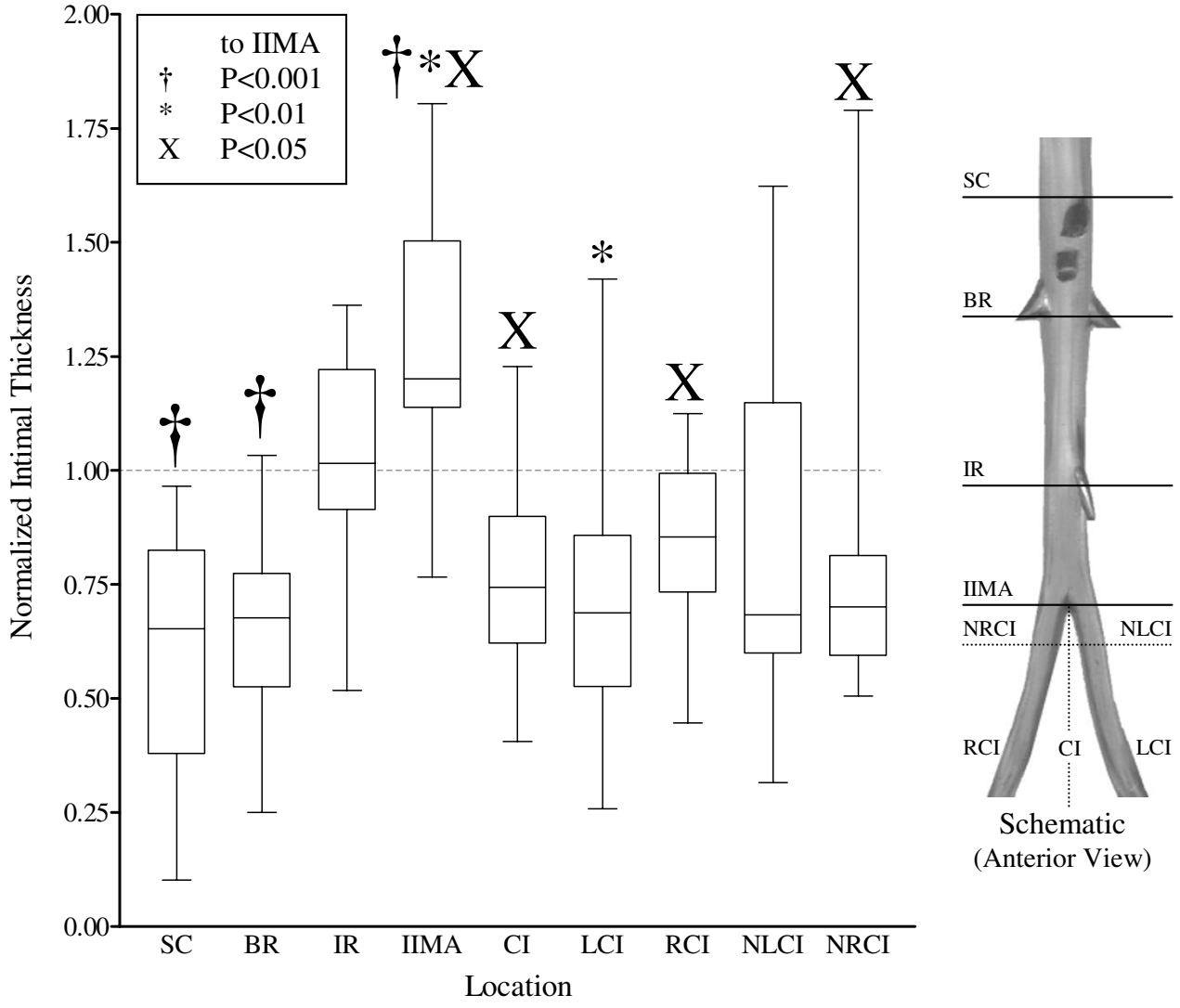

Figure 5
Normalized intimal thickness by (axial) location and selected P values from a Bonferroni's multiple comparison test. The boxes denote the range between lower and upper quartile. The horizontal lines within the boxes denote the median value and the whiskers the range of the data. IT normalization by patient-specific mean IT (BR, IR, and IIMA mean thickness). SC – Supraceliac, BR – Branch Region, IR – Infrarenal, IIMA – InfraIMA, CI – Mean of Common Iliacs, LCI – Left Common Iliac, RCI – Right Common Iliac, NLCI – Near Bifurcation LCI, NRCI – Near Bifurcation RCI. See Schematic. The supraceliac region is defined as the superior portion of the celiac branch point to 3.5 cm proximal of it. The NRCI and NLCI regions are subsets of the RCI and LCI regions and defined as the area in the common iliac arteries within 1.0 cm of the abdominal aortic bifurcation.

A further analysis evaluated the dependence of IT on axial position. The aortas for this purpose were divided into eight (axial) sections, as described above. In addition, all IT values for the individual samples were normalized by their patient-specific mean IT. This was done to avoid having the older subjects, which generally have thicker intimas, bias the data, and to thus allow comparison of the IT of different locations. The normalized IT data by axial location is given in Figure 5. A one-way ANOVA (assuming a parametric distribution) was done on the normalized data and followed by a Bonferroni multiple comparison test. The comparison found that the intima of

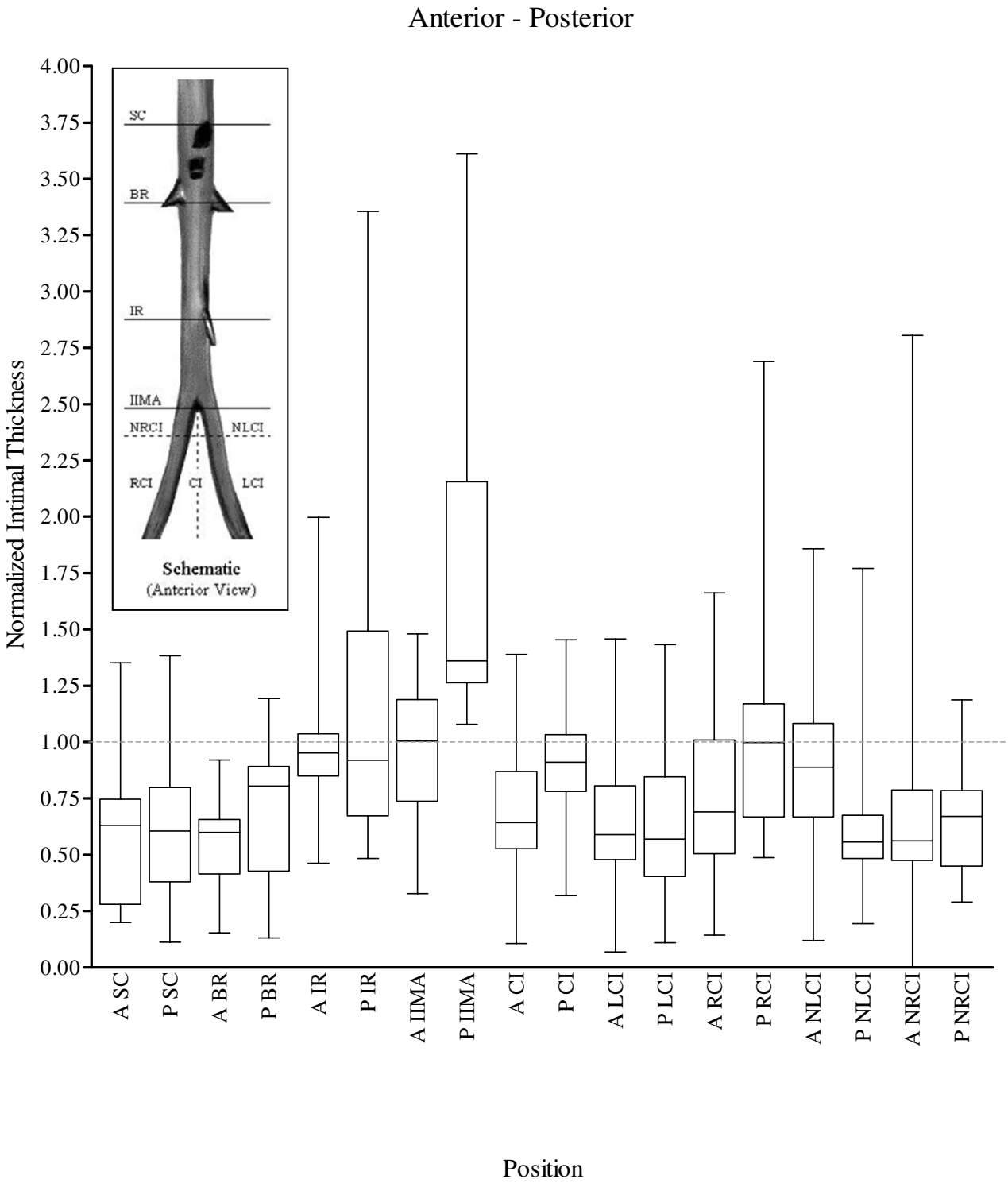

Figure 6
Box and whisker plot of the normalized intimal thickness by section and radial location (anterior/posterior). A – Anterior, P – Posterior, SC – Supraceliac, BR – Branch Region, IR – Infrarenal, IIMA – InfraIMA, CI – Mean of Common Iliacs, LCI – Left Common Iliac, RCI – Right Common Iliac, NLCI – Near Bifurcation LCI, NRCI – Near Bifurcation RCI. See Schematic. IT Normalization by patient-specific mean IT (BR, IR and IIMA mean thickness).

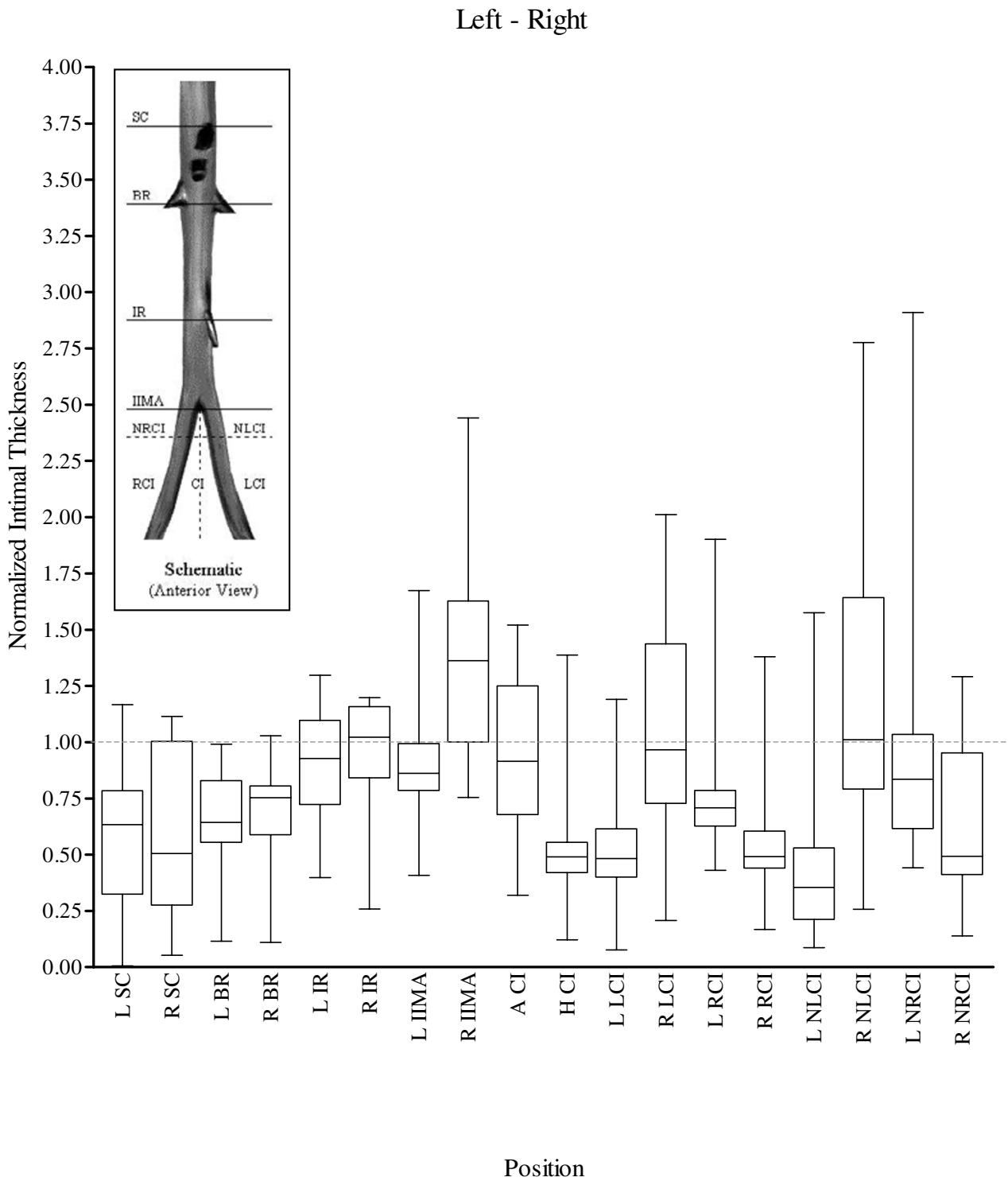

Figure 7
Box and whisker plot of the normalized intimal thickness by section and radial location (left/right). L – Left, R – Right. See Schematic and refer to Figure 6 for the definition of the abbreviations. IT normalization by patient-specific mean IT.

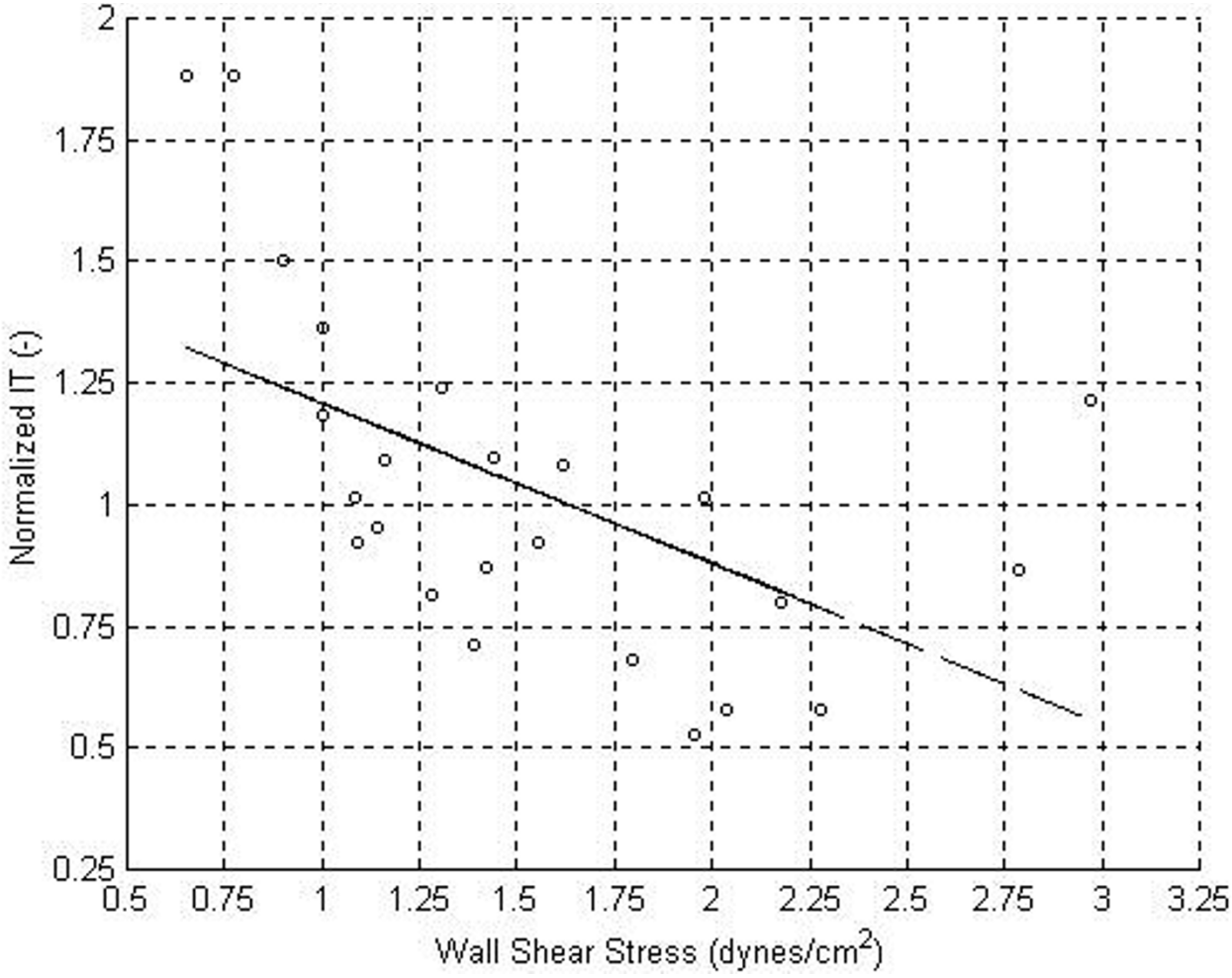

Figure 8
Normalized intimal thickness versus the *in vivo* wall shear stress for resting flow conditions. Regression line: y = -0.32*x+1.53; r^2 = 0.3099; P = 0.0047 (2-tailed).

the infraIMA section was statistically thicker than all sections, except the near bifurcation LCI section. Also, an analysis was done to determine whether IT differed significantly by axial and circumferential position. In this analysis the (axial) sections were each subdivided into four circumferential regions (anterior, posterior, left, right) and compared with an ANOVA and Bonferroni multiple comparison (Figure 6 and Figure 7). We found that the posterior infraIMA IT was significantly different from all circumferential locations of the branch region and supraceliac sections. The sections the posterior infraIMA did not differ statistically from the anterior infrarenal, posterior infrarenal, right infraIMA, posterior RCI, right LCI, left near bifurcation RCI, and right near bifurcation LCI.

Wall Shear Stress and Intimal Thickening

The relationship between the IT (measured in the autopsy samples) and the WSS (measured in the hemodynamic model) was examined under resting flow conditions. For this analysis the infrarenal, infraIMA, and common iliac regions (defined above) were split equally into proximal and distal sections and thus collectively defined 6 × 4 (axial × circumferential) regions. IT thickness data in the

iliacs was averaged to give one set of values. The WSS data was similarly subdivided and averaged within each subregion. Linear regression of regional (patient-specific mean IT value) normalized IT on regional WSS showed that increased IT was correlated with low WSS ($r^2 = 0.3099$; $P = 0.0047$ (2-tailed); Figure 8). The above analysis was repeated for mild exercise flow conditions, once again yielding a covariation of normalized IT and WSS that could not be explained by chance alone ($r^2 = 0.3692$; $P = 0.0016$). Linear regressions of normalized IT on axial spatial WSS gradient showed no correlation or statistically significant dependencies ($r^2 = 0.0033$, $P = 0.7891$ for the rest flow condition; $r^2 = 0.0106$, $P = 0.6318$ for the exercise flow condition (data not shown)).

Discussion

One of the contributions of this study is that it is the first to look at patient-specific hemodynamics in detail throughout the entire infrarenal human aorta. Other studies have looked at patient-specific models of the aorto-iliac bifurcation [31-33] or have looked at population-averaged models of the abdominal aorta [3,9,10]. Our results showed that patient-specific aortic geometrical features, such as the expansion at the IMA, strongly influence details of the WSS pattern. This is consistent with studies on a patient-specific abdominal aortic bifurcation model that showed significant asymmetry in the WSS pattern [32].

In our work, a key geometric factor was vessel cross-sectional area, which decreased from just inferior of the renal arteries to approximately three-fourths of the distance to the IMA. This was accompanied by an increase in WSS. Distal to this region, the cross-sectional area of the aorta increased and WSS decreased. A second important geometric factor was vessel curvature. Specifically, the slight curvature of the aorta in the IMA- abdominal aortic bifurcation region created an elevated WSS on the anterior wall and decreased WSS on the posterior wall. The differences in WSS between the iliac arteries can be accounted for by the smaller caliber and larger sagittal plane angle (with respect to the abdominal aorta terminus) that the left common iliac had compared to the right. The smaller WSS gradient at the flow divider during mild exercise can be accounted for by its similarity to flow entering a pipe from a large reservoir [34]. This analogy also provides some insight into why the LCI WSS pattern in mild exercise flow is characterized by smaller gradients in the Hagen-Poiseuille normalized WSS (data not shown); entrance flows at higher flow rates require greater development lengths.

Histomorphometry

The statistical analysis showed a positive correlation between patient-specific mean IT and age. Increasing IT with age is consistent with the belief that IT is a precondition for atherosclerosis [35,36], a disease that primarily afflicts the elderly [37]. An ANOVA comparing IT at different axial positions suggests that the infraIMA region of young individuals typically exhibits the thickest intima and is by extension likely susceptible to atherosclerotic lesion formation. A further analysis considered both axial and circumferential variation and found the region of highest IT to be the posterior wall of the infraIMA region.

The correlations between age and normalized IT suggest that the rates of intimal thickening of the supraceliac, branch region, and infraIMA sections change significantly relative to one another with age. More specifically, the normalized IT of the supraceliac and branch region sections was found to increase with age, while the normalized IT of the infraIMA section decreased with age. These findings suggest that the supraceliac and branch region sections thicken at a higher rate in older subjects than in younger subjects. Conversely, the infraIMA region thickens at a lower rate in older subjects than in younger subjects. The idea that hemodynamically-influenced intimal thickening depends on age has been previously suggested by others, such as Friedman et al. [22], who studied intimal thickening at the abdominal aortic bifurcation in patients of different ages.

Reasons for this age-dependence are not obvious. One possibility is that age could influence the biology of endothelial and mural smooth muscle cells and their response to hemodynamic stimuli. A second possibility is that the abdominal aorta's geometry changes with age, as documented by Fleischmann et al [13]. Hemodynamically significant changes include the disappearance with age of the expansion at the IMA, and changes in taper [13,38]. The importance of caliber change at the IMA can be seen by comparing WSS patterns from Taylor's study [9] (where the aorta did not show this expansion) to the results of this study.

Relationship Between Hemodynamics and Intimal Thickening

Although patient-specific geometric features do influence the details of WSS patterns, many large-scale hemodynamic features are common to all infra-renal aortas. For example, we observe high shear stresses on the aorto-iliac flow divider, lower shear stresses on the hips (wall opposite of flow divider) of this bifurcation, and a local minimum in WSS slightly inferior to the IMA due to caliber changes in the aorta. Another common feature is that aortic curvature causes WSS on the posterior wall in the infraIMA region to be lower than on the anterior wall in the same region, as reported by Long et al. [32], as well as this study. This commonality of large-scale hemodynamic features allows us to extract useful information by investi-

gating relationships between our hemodynamic measurements and our patient-averaged IT measurements.

Our data show that there is a statistically significant inverse correlation between WSS and intimal thickening, both under resting and exercise conditions. This supports the belief that low WSS leads to IT and possibly is atherogenic as suggested by Caro [21], and is consistent with work from Pedersen [39,40]. It is also supported by the observation that intimal thickening at the posterior IMA was statistically significantly larger than elsewhere in the infrarenal aorta. This region has the lowest WSS found in the flow model. These conclusions differ somewhat from inferences drawn from the pattern of lesions suggested by Cornhill et al. [41]. In particular, the anterior infrarenal region in the Cornhill study is a high probability area. The reason for the difference is not clear but, may be a result of the different methods used, i.e. sudanophilic staining vs. intimal thickness measurements.

Limitations

No patient-specific correlations could be done, since WSS was measured in a model of a healthy human's aorta and compared with IT in unrelated autopsy samples. This study made several simplifications. Differentiation between adaptive intimal thickening [42] and atherosclerotic intimal thickening was not possible in this study due to the limited number of autopsy samples and also because the histologic sections were stained mainly for morphometric analysis. Further, blood was assumed to be Newtonian, the aorta rigid, the flow steady and the flow exiting the major branches of the aorta of secondary importance. None of these significantly influence the trends in the data. Dutta and Tarbell suggested Newtonian fluid rheology results in an error of approximately 10% in the WSS [43]. Hayashi showed that the wall motion has a small effect on WSS [31]. It is well known that the flow typically reverses on the posterior InfraIMA wall and at the hips of the abdominal aortic bifurcation during diastole [6,44]. Non-steady flow patterns have been suggested to influence IT [6,45]. These factors remain to be studied in patient-specific models. Studies by Myers et al [23] and Bonert et al [46] in other geometries suggest unsteady flow WSS patterns are similar to those from steady flow [23,46]. Lastly, a study in the pig suggests branch flow is important if the flow is also assumed to be steady [47]. However, work by Myers et al. [23], for small branches, and Taylor et al. [10], for large branches, suggest the main effect of the branch flow is restricted to the region close to the branch. The data of Taylor et al., when normalized by the IMA Hagen-Poiseuille WSS, suggests that the branch flow influences only the first two centimeters from the renal branch points because the differences between rest flow and mild exercise flow thereafter are relatively small. This is despite the fact that the renal to suprarenal flow ratio is 0.46 (0.80 L/min / 1.73 L/min) and 0.19 (0.69 L/min / 3.54 L/min) for rest and mild exercise respectively. The reason the renal flow is likely not significant further downstream is possibly explained by the gradual taper of the aorta at the renal arteries. Nevertheless, both of these factors should be investigated further in humans.

Conclusions

Local geometrical features, such as the expansion at the IMA in the patient-specific model studied, influence WSS patterns. IT increases with age and regions change significantly in thickness relative to one another with age. Also, rates of intimal thickening in the abdominal aorta are possibly influenced by age related geometrical changes. If the anatomically faithful patient-specific model examined is typical for young patients, low WSS on the posterior wall inferior to the inferior mesenteric artery coincides with the region of most prominent IT. An examination of patients of various ages may further our understanding of atherosclerotic lesion development. Matching patients with models representative of their ages may be sufficient for reproducing the primary hemodynamic features of their abdominal aortas. Future work could match patient models with their histomorphology.

Authors' Contributions

MB constructed the transparent flow model, did the statistical analysis, and drafted the manuscript. RLL participated in the analysis of the flow experiments and autopsy data. JB participated in the collection and processing of the autopsy samples. CRE, KWJ and MO participated in the design of the study. JGM carried out the reconstruction of the flow model geometry from the CT images. All authors read and approved the final manuscript.

Acknowledgements

Ms. Yan Kiu Chan constructed the computer model of the abdominal aorta geometry studied. This work was supported in part by a Natural Sciences and Engineering Research Council of Canada Scholarship (MB), the R. Fraser Elliott Chair in Vascular Surgery, and the Canada Research Chair in Computational Technology (CRE). Franz Schuh is thanked for his great assistance in the construction of the transparent flow model. Heart and Stroke Foundation of Ontario – NA 5007 (MO, JB).

References

1. Ku DN, Glagov S, Moore JE, Zarins CK: **Flow patterns in the abdominal aorta under simulated postprandial and exercise conditions: an experimental study.** *J Vasc Surg* 1989, **9:**309-316.
2. Moore JE, Ku DN: **Wall shear stress measurements in a model of the human abdominal aorta using magnetic resonance imaging.** *Advances in Bioengineering, ASME Proceedings* 1991, **20:**375-377.
3. Moore JE, Ku DN, Zarins CK, Glagov S: **Pulsatile flow visualization in the abdominal aorta under differing physiologic conditions: implications for increased susceptibility to atherosclerosis.** *J Biomech Eng* 1992, **114:**391-397.
4. Moore JE, Ku DN: **Pulsatile velocity measurements in a model of the human abdominal aorta under simulated exercise and postprandial conditions.** *J Biomech Eng* 1994, **116:**107-111.

5. Moore JE, Maier SE, Ku DN, Boesiger P: **Hemodynamics in the abdominal aorta: a comparison of in vitro and in vivo measurements.** *J Appl Physiol* 1994, **76:**1520-1527.
6. Moore JE, Ku DN: **Pulsatile velocity measurements in a model of the human abdominal aorta under resting conditions.** *J Biomech Eng* 1994, **116:**337-346.
7. Moore JE, Xu C, Glagov S, Zarins CK, Ku DN: **Fluid wall shear stress measurements in a model of the human abdominal aorta: oscillatory behavior and relationship to atherosclerosis.** *Atherosclerosis* 1994, **110:**225-240.
8. Shipkowitz T, Rodgers VG, Frazin LJ, Chandran KB: **Numerical study on the effect of steady axial flow development in the human aorta on local shear stresses in abdominal aortic branches.** *J Biomech* 1998, **31:**995-1007.
9. Taylor CA, Hughes TJ, Zarins CK: **Finite element modeling of three-dimensional pulsatile flow in the abdominal aorta: relevance to atherosclerosis.** *Ann Biomed Eng* 1998, **26:**975-987.
10. Taylor CA, Hughes TJ, Zarins CK: **Effect of exercise on hemodynamic conditions in the abdominal aorta.** *J Vasc Surg* 1999, **29:**1077-1089.
11. Lee YT, Keitzer WF, Watson FR, Liu H: **Vascular geometry at the abdominal aortic bifurcation.** *J Am Med Womens Assoc* 1982, **37:**77-81.
12. Bargeron CB, Hutchins GM, Moore GW, Deters OJ, Mark FF, Friedman MH: **Distribution of the geometric parameters of human aortic bifurcations.** *Arteriosclerosis* 1986, **6:**109-113.
13. Fleischmann D, Hastie TJ, Dannegger FC, Paik DS, Tillich M, Zarins CK *et al.*: **Quantitative determination of age-related geometric changes in the normal abdominal aorta.** *J Vasc Surg* 2001, **33:**97-105.
14. Pearce WH, Slaughter MS, LeMaire S, Salyapongse AN, Feinglass J, McCarthy WJ *et al.*: **Aortic diameter as a function of age, gender, and body surface area.** *Surgery* 1993, **114:**691-697.
15. Pedersen OM, Aslaksen A, Vik-Mo H: **Ultrasound measurement of the luminal diameter of the abdominal aorta and iliac arteries in patients without vascular disease.** *J Vasc Surg* 1993, **17:**596-601.
16. Davies PF: **Flow-mediated endothelial mechanotransduction.** *Physiol Rev* 1995, **75:**519-560.
17. Gimbrone MA Jr, Topper JN, Nagel T, Anderson KR, Garcia-Cardena G: **Endothelial dysfunction, hemodynamic forces, and atherogenesis.** *Ann N Y Acad Sci* 2000, **902:**230-239.
18. Nerem RM, Alexander RW, Chappell DC, Medford RM, Varner SE, Taylor WR: **The study of the influence of flow on vascular endothelial biology.** *Am J Med Sci* 1998, **316:**169-175.
19. Asakura T, Karino T: **Flow patterns and spatial distribution of atherosclerotic lesions in human coronary arteries.** *Circ Res* 1990, **66:**1045-1066.
20. Ojha M: **Wall shear stress temporal gradient and anastomotic intimal hyperplasia.** *Circ Res* 1994, **74:**1227-1231.
21. Caro CG, Fitz-Gerald JM, Schroter RC: **Atheroma and arterial wall shear. Observation, correlation and proposal of a shear dependent mass transfer mechanism for atherogenesis.** *Proc R Soc Lond B Biol Sci* 1971, **177:**109-159.
22. Friedman MH, Deters OJ, Bargeron CB, Hutchins GM, Mark FF: **Shear-dependent thickening of the human arterial intima.** *Atherosclerosis* 1986, **60:**161-171.
23. Myers JG, Ojha M, Johnston KW, Ethier CR: **Influence of Branches, Curvature and Caliber on Blood Flow Patterns in the Human Right Coronary Artery.** *Submitted to Computer Methods in Biomechanics and Biomedical Engineering* 2001.
24. Kirpalani A, Park H, Butany J, Johnston KW, Ojha M: **Velocity and wall shear stress patterns in the human right coronary artery.** *J Biomech Eng* 1999, **121:**370-375.
25. Park H, Moore JA, Trass O, Ojha M: **Laser photochromic velocimetry estimation of the vorticity and pressure field – two-dimensional flow in a curved vessel.** *Experiments in Fluids* 1999, **26:**55-62.
26. Leask RL: *Intimal Thickening and Hemodynamics of Human Coronary Artery Bypass Grafts University of Toronto*; 2002. Ph.D.
27. Caro CG, Pedley TJ, Schroter RC, Seed WA: *Mechanics of Circulation New York: Oxford University Press*; 1978.
28. Park H: *Flow Field Measurements in the Plane of Symmetry of a 90° Curved Vessel Using Laser Photochromic Velocimetry University of Toronto*; 1998. Ph.D.
29. Ethier CR, Prakash S, Steinman DA, Leask RL, Couch GG, Ojha M: **Steady flow separation patterns in a 45 degree junction.** *J Fluid Mech* 2000, **411:**1-38.
30. Ojha M: **Spatial and temporal variations of wall shear stress within an end-to-side arterial anastomosis model.** *J Biomech* 1993, **26:**1377-1388.
31. Hayashi K, Yanai Y, Naiki T: **A 3D-LDA study of the relation between wall shear stress and intimal thickness in a human aortic bifurcation.** *J Biomech Eng* 1996, **118:**273-279.
32. Long Q, Xu XY, Bourne M, Griffith TM: **Numerical study of blood flow in an anatomically realistic aorto-iliac bifurcation generated from MRI data.** *Magn Reson Med* 2000, **43:**565-576.
33. Friedman MH, Hutchins GM, Bargeron CB, Deters OJ, Mark FF: **Correlation between intimal thickness and fluid shear in human arteries.** *Atherosclerosis* 1981, **39:**425-436.
34. White FM: *Fluid Mechanics* 3rd edition. *Toronto: McGraw-Hill Inc*; 1994.
35. Ross R, Glomset JA: **The pathogenesis of atherosclerosis (first of two parts).** *N Engl J Med* 1976, **295:**369-377.
36. Ross R, Glomset JA: **The pathogenesis of atherosclerosis (second of two parts).** *N Engl J Med* 1976, **295:**420-425.
37. Tilson MD, Stansel HD: **Differences in results for aneurysms vs occlusive disease after bifurcation grafts: results of 100 elective grafts.** *Arch Surg* 1980, **115:**1173-1175.
38. Sundell PM, Roach MR: **The role of taper on the distribution of atherosclerosis in the human infra-renal aorta.** *Atherosclerosis* 1998, **139:**123-129.
39. Pedersen EM, Agerbaek M, Kristensen IB, Yoganathan AP: **Wall shear stress and early atherosclerotic lesions in the abdominal aorta in young adults.** *Eur J Vasc Endovasc Surg* 1997, **13:**443-451.
40. Pedersen EM, Oyre S, Agerbaek M, Kristensen IB, Ringgaard S, Boesiger P *et al.*: **Distribution of early atherosclerotic lesions in the human abdominal aorta correlates with wall shear stresses measured in vivo.** *Eur J Vasc Endovasc Surg* 1999, **18:**328-333.
41. Cornhill JF, Herderick EE, Stary HC: **Topography of human aortic sudanophilic lesions.** *Monogr Atheroscler* 1990, **15:**13-19.
42. Stary HC, Blankenhorn DH, Chandler AB, Glagov S, Insull W Jr, Richardson M *et al.*: **A definition of the intima of human arteries and of its atherosclerosis-prone regions. A report from the Committee on Vascular Lesions of the Council on Arteriosclerosis, American Heart Association.** *Circulation* 1992, **85:**391-405.
43. Dutta A, Tarbell JM: **Influence of non-Newtonian behavior of blood on flow in an elastic artery model.** *J Biomech Eng* 1996, **118:**111-119.
44. Mostbeck GH, Dulce MC, Caputo GR, Proctor E, Higgins CB: **Flow pattern analysis in the abdominal aorta with velocity-encoded cine MR imaging.** *J Magn Reson Imaging* 1993, **3:**617-623.
45. Ku DN, Giddens DP, Zarins CK, Glagov S: **Pulsatile flow and atherosclerosis in the human carotid bifurcation. Positive correlation between plaque location and low oscillating shear stress.** *Arteriosclerosis* 1985, **5:**293-302.
46. Bonert M, Myers JG, Fremes S, Williams J, Ethier CR: **A Numerical Study of Blood Flow in CABG Side-to-Side Anastomoses.** *Ann Biomed Eng* 2002, **30:**599-611.
47. Clingan PA, Friedman MH: **The effect of celiac and renal artery outflows on near-wall velocities in the porcine iliac arteries.** *Ann Biomed Eng* 2000, **28:**302-308.